Controlled modification of resonant tunneling in metal-insulator-insulator-metal structures

I.Z. Mitrovic,[1,a)] A.D. Weerakkody,[1,b)] N. Sedghi,[1] J.F. Ralph,[1] S. Hall,[1] V.R. Dhanak,[2] Z. Luo,[3,c)] and S. Beeby[3]

[1]*Department of Electrical Engineering & Electronics, University of Liverpool, Liverpool L69 3GJ, UK*

[2]*Department of Physics and Stephenson Institute for Renewable Energy, University of Liverpool, Liverpool L69 7ZF, UK*

[3]*Department of Electronics and Computer Science, University of Southampton, Southampton, SO17 1BJ, UK*

[a)]Author to whom correspondence should be addressed. Electronic mail: ivona@liverpool.ac.uk

[b)]Now at Department of Electrical, Computer, and Energy Engineering, University of Colorado, Boulder, CO 80309-0425, USA.

[c)]Now at School of Water, Energy and Environment, Cranfield University, Cranfield MK43 0AL, UK.

Abstract

We present comprehensive experimental and theoretical work on tunnel-barrier rectifiers comprising bilayer (Nb_2O_5/Al_2O_3) insulator configurations with similar (Nb/Nb) and dissimilar (Nb/Ag) metal electrodes. The electron affinity, valence band offset and metal work function were ascertained by X-ray photoelectron spectroscopy, variable angle spectroscopic ellipsometry and electrical measurements on fabricated reference structures. The experimental band line-up parameters were fed into a theoretical model to predict available bound states in the Nb_2O_5/Al_2O_3 quantum well and generate tunneling probability and transmittance curves under applied bias. The onset of strong resonance in the sub-V regime was found to be controlled by a work function difference of Nb/Ag electrodes in agreement with the experimental band alignment and theoretical model. A superior low-bias asymmetry of 35 at 0.1 V and responsivity of 5 A/W at 0.25 V were observed for Nb/4 nm Nb_2O_5/1 nm Al_2O_3/Ag structure, sufficient to achieve rectification of over 90% of the input alternate current terahertz signal in a rectenna device.

Key words: resonant tunneling, metal-insulator-metal diodes, band line-up, bound states, rectification

This manuscript was accepted by Appl. Phys. Lett. Click here to see the version of record.

Effective control of quantum mechanical tunneling through an ultrathin dielectric represents a fundamental materials challenge in the quest for high performance metal/insulator (M/I) based diodes.[1,2] Metal-Insulator-Metal (MIM) diodes are contenders as rectifiers in rectennas (rectifying antennas) due to their high-speed operation, low fabrication cost, well-established high-k dielectric technology, and ease of integration with broad-band patch antennas.[3] The rectifier is the most challenging part of rectenna implementation. It is to be designed to operate at terahertz (THz)/infrared frequencies and above. The operation speed of MIM diodes depends on the tunneling transmission time, typically in the range of femtoseconds,[4] and theoretically can reach to a few 100 THz or even into the range of the solar spectrum.[3] Structures with two or more dielectric layers as metal-insulator-insulator-metal (MI^2M) or metal-insulator-insulator-insulator-metal (MI^3M) benefit from resonant tunneling (RT)[5,6] which increases the device nonlinearity leading to a high degree of rectification. The limiting parameter for small signal rectification is the turn-on voltage (V_{ON}) of these diodes, defined as a point where the tunneling current is significantly increased by resonance. The turn-on voltage in reported devices is very large, usually a few volts[5-10] being beyond the small signal amplitude. Applying a direct current (dc) bias to the diode is not practical in this design since the dc power to bias the diode at V_{ON} would be much greater than that achieved by rectification of the alternate current (ac) signal in the energy harvesting application. Hence, it is vital to design the device structure to bring substantial nonlinearity close to zero volts.

The resonant tunneling has been reported at 1.3 V and 2.7 V for triple cascaded insulator $MI_1I_2I_3M$ structures based on $Cr/Al_2O_3/HfO_2/Cr_2O_3/Cr$,[6] but not on double insulator MI^2M structures.[9] No asymmetry (η) and nonlinearity or responsivity (R) have been reported for voltages below 0.5 V.[6,9] The resonant tunneling has been predicted for $W/Nb_2O_5/Ta_2O_5/W$ structure, however not experimentally demonstrated.[5] In the case of bilayer MI^2M structures with substantial work function (WF) difference between dissimilar electrodes of 0.6 eV (ZCAN/Al)[7,8] and 0.65 eV (Ni/Cr),[11] the highest asymmetry reported < 0.8 V is $10^{7,8}$ and 16 at 0.5 V.[11] We have recently reported superior low-bias asymmetry (18 @ 0.35 V) and responsivity (9 A/W @ 0.2 V) for $Al/Ta_2O_5/Al_2O_3/Al$ and $Al/Nb_2O_5/Al_2O_3/Al$ devices respectively[12] as well as enhanced rectification for $Al/Ta_2O_5/Al_2O_3/Cr$ at V_{ON} = 0.32 V.[13] In this letter, we report resonant tunneling in $Nb/Nb_2O_5/Al_2O_3/Nb$ rectifier in sub-V regime and its modification by introducing a dissimilar metal electrodes (Nb/Ag) device configuration.

The devices were fabricated on 4 cm × 4 cm Corning glass substrates with an rms (root mean square) surface roughness of 0.32 ± 0.07 nm. The metals of 60 nm nominal thickness were deposited by thermal evaporation (Al and Ag) and by dc sputtering (Nb). The electrodes were defined by conventional photolithography or a shadow mask. The oxides were deposited by radio frequency (rf) sputtering using rates of 0.006 nm/s at

This manuscript was accepted by Appl. Phys. Lett. Click here to see the version of record.

140 W for Al_2O_3, 0.045 nm/s at 100 W for Ta_2O_5 and 0.03 nm/s at 70 W for Nb_2O_5. The sputtering time was adjusted to obtain films of different target (nominal) thicknesses. The reference samples of thin (3-5 nm, referred to as interfacial) and thick (10-20 nm, referred to as bulk) oxides (Nb_2O_5, Al_2O_3, Ta_2O_5) were fabricated on 50 nm SiO_2/Si substrates using the same rf sputtering conditions as the films in MIM and MI^2M devices. These samples were used to ascertain the optical properties and band gap by variable angle spectroscopy ellipsometry (VASE), and band line-up by X-ray photoelectron spectroscopy (XPS). The XPS was performed under normal emission in a standard ultra-high vacuum system consisting of a PSP Vacuum Technology dual anode (Mg/Al) X-ray source and a hemispherical electron energy analyser equipped with five channeltrons. The spectrometer was calibrated so the Ag $3d_{5/2}$ photoelectron line had a binding energy (BE) of 368.35 eV and a full width at half maximum (FWHM) of 0.8 eV being the overall spectral resolution for this study. The XPS core level (CL) spectra were calibrated by setting the C 1s at 284.6 eV for all samples. A Shirley-type background was used for the fitting of all spectra. The CL positions are defined by fitting a Voigt curve to the measured peaks, which introduces typically error of ± 0.08 eV. The error bar (± 0.2 eV) defined from XPS is due to valence band maximum (VBM) estimation through the linear interpolation method. To extract the barrier height at the M/I interface, the single insulator MIM devices with nominal 5 nm Nb_2O_5 (or Ta_2O_5) films were fabricated using Al, Nb and Ag electrodes. The MI^2M device structures comprised of 4 nm Nb_2O_5/1 nm Al_2O_3 patterned with Nb/Nb and Nb/Ag electrodes and device area of 100 μm × 100 μm. There was a variation of nominal thickness for processed devices, 4.54 nm Nb_2O_5/1.15 nm Al_2O_3 as determined by VASE (± 0.1 nm).

Fig. 1(a) depicts extraction of the binding energy difference (δ) of secondary electrons cut-off and valence band maximum from the XPS spectra for bulk Al_2O_3 (top) and Nb_2O_5 (bottom) samples. The ionization potential is determined as IP (eV) = hν – (δ + qV_{app}), where hν = 1253.6 eV and qV_{app} = 10 eV, yielding the values of 8 eV for Al_2O_3 and 7.49 eV for Nb_2O_5. The electron affinity can then be calculated using χ = IP – E_g, where the band gap (E_g) of Al_2O_3 and Nb_2O_5 have been found to be 6.43 eV[14] and 3.77 eV[12] by VASE in agreement with the literature.[15,16] Hence, the electron affinity measured for Al_2O_3 and Nb_2O_5 is 1.57 eV and 3.72 eV (± 0.2 eV) respectively. The valence band offset (VBO) between Nb_2O_5 and Al_2O_3 was derived from Kraut's method[17] using the equation VBO = δ(Al_2O_3) – δ(Nb_2O_5) + δ_{int}, where δ(Al_2O_3) refers to the BE difference of Al $2p_{5/2}$ CL and VBM for bulk Al_2O_3 (Fig. 1(b), bottom), δ_{int} of Nb $3d_{5/2}$ and Al $2p_{3/2}$ CLs for interfacial Nb_2O_5/Al_2O_3 sample (Fig. 1(b), middle), and δ(Nb_2O_5) of Nb $3d_{5/2}$ CL and VBM for bulk Nb_2O_5 sample (Fig. 1(b), top). No additional interface components were observed from fitting Nb 3d and Al 2p CLs of interfacial 3.8 nm Nb_2O_5/Al_2O_3 sample (Fig. 1(b), middle). The FWHM of Al $2p_{3/2}$ and Nb $3d_{5/2}$ CLs are found to be in the range of 1.4-1.5 eV. Using the estimated values from Fig. 1(b), the

VBO = 0.48 ± 0.2 eV. It is worth pointing that two independent measurements confirm the same conduction band offset (CBO) between Nb_2O_5 and Al_2O_3 within the experimental error: (i) from electron affinity CBO = $\chi(Nb_2O_5)$ - $\chi(Al_2O_3)$ = 2.15 eV (Fig. 1(a)), and (ii) from VBO and Kraut's method CBO = $E_g(Al_2O_3)$ – VBO – $E_g(Nb_2O_5)$ = 2.18 eV (Fig. 1(b)).

Fig. 2(a) shows Fowler-Nordheim (FN) plots for MIM reference diodes, while the insets depict the schematics of extracted M/I barrier heights. A linear relationship between $\ln(J/E_{ox}^2)$ and $(1/E_{ox})$ can be seen, with an $R^2 > 0.999$, being indicative of an excellent fit[16] and the dominance of FN tunneling (FNT) over the bias range. The barrier height at the M/I interface was extracted from the slope of FNT plots being equal to $-\frac{4\sqrt{2m^*}(q\phi_b)^{3/2}}{3q\hbar}$, where q is electronic charge, $\hbar = h/2\pi$ is Plank's constant, $m^* = 0.5 \times m_0$ is effective mass, m_0 is electron mass, and ϕ_b - barrier height. Note that there are no consistent data available for the effective mass of thin oxides and values reported in the literature vary from (0.45-1) × m_0,[18] 0.28 × m_0,[19] 0.42 × m_0,[20] 0.5 × m_0,[21] 1 × m_0.[5,22] It is worth mentioning that the variation of m* from 0.1 to 1 (× m_0) in this work, results in barrier height variation of ± 0.08 eV, being well within the experimental error of band line-up estimation (± 0.2 eV). The extracted barrier heights from Fig. 2(a) are 0.39 eV for Nb/Nb_2O_5, 0.56 eV for Al/Nb_2O_5, 0.72 eV for Ag/Ta_2O_5 and 0.74 eV for Al/Ta_2O_5. The work function of the metals is then determined using WF = $\chi + \phi_b$, resulting in 4.11 eV for Nb and 4.28 eV for Al. Since the MIM reference structure of Ag/Nb_2O_5/Ag did not produce valid (linear) FNT plots, the data from Ag/Ta_2O_5/Ag and Al/Ta_2O_5/Al were used (see right-side plots in Fig. 2(a)) to first indirectly determine $\chi(Ta_2O_5)$ = WF(Al) - ϕ_b(Al/Ta_2O_5) = 3.54 eV. Then, the WF(Ag) = $\chi(Ta_2O_5) + \phi_b$(Ag/Ta_2O_5) = 4.26 eV. In summary of the band line-up study, Fig. 2(b) depicts the experimental values measured in this work, which are used as input parameters for the theoretical study of resonant tunneling in MI^2M structures shown in Fig. 3.

A model for calculating the bound states in a quantum well has been previously reported[5,23-28] and was used to generate the data in Fig. 3. The model is based on a modified multi-barrier Tsu-Esaki method,[29,30] whereby the insulator stack is assumed to consist of multiple slices with different barrier heights. The transmission amplitude at each energy level is found by solving the time-independent Schrödinger equation[26] using the transmission matrix method.[30] Fig. 3 depicts energy band diagrams of Nb/Nb_2O_5/Al_2O_3/Nb structure under bias of 0.5 V (Fig. 3(a)) and 1 V (Fig. 3(b)) applied to the right Nb electrode. A quantum well is built between Nb_2O_5 and Al_2O_3. The model predicts two bound states: at 0.23 eV and 0.39 eV for 0.5 V; and at 0.01 eV and 0.22 eV for 1 V (see dashed horizontal lines in Figs. 3(a)-(b)). These states can be observed as sharp resonant peaks on tunneling probability curves shown in Figs.

This manuscript was accepted by Appl. Phys. Lett. Click here to see the version of record.

3(g)-(d). The other peaks of more rounded shape refer to free running states at Eigen energies. The transmittance curves are generated as the product of tunneling probability and Fermi-Dirac function, which defines the density of occupied and empty states at each metal contact. A substantial decrease of transmittance for 0.5 V can be observed in Fig. 3(c) due to both bound states being above the Fermi level of Nb left contact causing a significant reduction of the resonance peaks by the Fermi-Dirac function. Although the tunneling probability is much higher at 0.5 V than at −0.5 V bias, this is not the case for the transmittance. The current is calculated by integration of transmittance in energy, and is found to be at −0.5 V nearly twice of that at 0.5 V. This suggests that the number of electrons at the energy level of the bound states is small. The scenario changes when the bias is increased to 1 V (Fig. 3(d)). Here, both tunneling probability and transmittance have sharp peaks (resonance is close to Fermi level of left Nb contact) and as a result the current at 1 V is ~1.5× higher than that at −1 V. The rate of increase in current has become larger due to resonant tunneling in this case, and theoretically overcomes the current at negative bias at a voltage of 0.88 V termed as rectification reversal. This phenomenon was investigated further by fabricating this MI^2M device.

Fig. 4(a) shows current density (J) vs. voltage (V) characteristics for fabricated 4 nm Nb_2O_5/ 1 nm Al_2O_3 diodes with Nb/Nb and Nb/Ag electrodes. A sharp increase of current and a change of curvature can be observed from JV curves at ~ 0.7 V for Nb/Nb device and at ~0.9 V for Nb/Ag device. The large signal rectification is ascribed to the device asymmetry defined as the ratio of current at positive (I_+) or negative (I_-) bias, whichever larger, to that at opposite bias i.e. $\eta = |I_+/I_-|$ or $|I_-/I_+|$ and is shown in Fig. 4(b). A measure of small signal nonlinearity is responsivity (Fig. 4(c)), defined as the ratio of dc rectified current (I_{dc}) to input ac power (P_{in}), i.e. $R = I_{dc}/P_{in} = (I''/2I')|_{Vp}$,[31] where I' and I'' are the first and second derivatives of current at operating point V_p. There is a clear trend of enhanced asymmetry after the onset of resonant tunneling in Fig. 4(b), however the effect is weak: just above 1 for Nb/Nb device and up to 10 for Nb/Ag device. The former agrees with the model (see Fig. 3(c) and Fig. 4(b) bottom). Interestingly, a superior asymmetry ($|I_-|/|I_+|$) of 35.2 at low bias of 0.06 V can be observed for Nb/Ag device, however this is not due to the effect of RT. This phenomenon requires further investigation and could be related to trapped charge in Al_2O_3 layer. The peak device responsivities are found to be 5 A/W at 0.25 V and 8 A/W at 1.1 V for Nb/Ag device and 2 A/W at 0.05 V for Nb/Nb device (Fig. 4(c)).

As can be seen in Fig. 2(b), the work function of Ag is 0.15 eV larger than that of Nb. Hence the Nb/Ag device is not in the flat band condition at zero bias (Fig. 5(a)), and requires an external bias of ~0.2 V to reach it (Fig. 5(b)). Therefore, a larger voltage must be applied on this structure to form a quantum well compared to the Nb/Nb device. The first bound state forms at 0.41 eV at 0.5 V. However, there is no

This manuscript was accepted by Appl. Phys. Lett. Click here to see the version of record.

evidence of RT in Fig. 4(a) at 0.5 V due to the large energy difference between the bound state and the Nb Fermi level (Figs. 3(a) and 5(c)). The conduction is dominated by direct tunneling (DT) up to 0.8 V, until Nb_2O_5 reaches the FNT regime (Fig. 5(d)). We have seen no evidence of Poole-Frenkel or trap-assisted tunneling in fabricated structures.[32] The RT kicks off from ~0.9 V (Fig. 4(a)) due to more electrons being available at the energy levels of two available bound states at 0.07 eV and 0.27 eV as shown in Fig. 5(e). It is evident from Fig. 4(a) that the rectification reversal shifts towards larger voltages (0.9 V) compared to $Nb/Nb_2O_5/Al_2O_3/Nb$ structure (0.7 V) due to band line-up depicted in Figs 5(a)-(e). The conduction in reverse bias is a combination of DT and FNT when the applied bias is smaller than –0.6 V (Fig. 5(f)). Further increase in the reverse bias beyond –0.6 V causes the Nb Fermi level to align with the CB edge of Nb_2O_5 as shown in Fig. 5(g) and the device reaches the so-called step tunneling (ST) regime.[5,7] It is worth mentioning that the theoretically predicted value of rectification reversal for $Nb/Nb_2O_5/Al_2O_3/Nb$ device is 0.88 V, while the experimentally observed value is 0.7 V. This is due to the actual thickness of Nb_2O_5 being ~0.5 nm higher than the nominal value of 4 nm used in the model in Fig. 3; hence the portion of potential applied on 4.5 nm Nb_2O_5 becomes larger and results in the formation of the quantum well at smaller voltages.

In summary, we have fabricated high-quality bilayer 4 nm Nb_2O_5/1 nm Al_2O_3 rectifiers based on similar (Nb/Nb) and dissimilar (Nb/Ag) electrodes. The quantum mechanical tunneling has been shown to dominate the conduction with the clear shift of the onset of resonant tunneling from 0.7 to 0.9 V due to the metal work function difference. This confirms that the controlled modification of resonant tunneling in MI^2M diodes is feasible. A superior low-bias asymmetry of 35 at 0.1 V and responsivity of 5 A/W at 0.25 V have been observed for Nb/Ag device structure. Although such asymmetry would allow to have over 90% of the input ac signal rectified in a rectenna device, challenges for implementation of this rectifier remain due to a time constant being much higher than required 10^{-15} s. The necessary advancements are needed in engineering lower M/I barrier and scaling device area in nanometer range to achieve rectifier for practical applications.

Acknowledgement. The work benefited from the funding of the EPSRC (UK) project no. EP/K018930/1 as well as Zepler Institute Research Collaboration Stimulus Fund, UK. The authors thank Dr D. Hesp for assistance in setting the equipment and measuring electron affinity from XPS secondary electrons spectra.

References

[1]G. Moddel, p. 1; S. Grover and G. Moddel, in *Rectenna Solar Cells* (Springer, New York, 2013), p. 25.

[2]S. Grover and G. Moddel, IEEE J. Photovoltaics **1**(1), 78 (2011).

[3]S. Hall, I. Z. Mitrovic, N. Sedghi, Y. C. Shen, Y. Huang, and J. F. Ralph, in *Functional Nanomaterials and Devices for Electronics, Sensors and Energy Harvesting* (Springer, Switzerland, 2014).

[4]T.E. Hartman, J. Appl. Phys. **33**, 3427 (1962).

[5]S. Grover and G. Moddel, Solid-State Electron. **67**, 94 (2012).

[6]P. Maraghechi, A. Foroughi-Abari, K. Cadien, and A. Y. Elezzabi, Appl. Phys. Lett. **100**, 113503 (2012).

[7]N. Alimardani and J. F. Conley, Appl. Phys. Lett. **102**, 143501 (2013).

[8]N. Alimardani, E. W. Cowell III, J. F. Wager, J. F. Conley, Jr., D. R. Evans, M. Chin, S. J. Kilpatrick, and M. Dubey, J. Vac. Sci. Technol. **A 30**, 01A113-1 (2012).

[9]P. Maraghechi, A. Foroughi-Abari, K. Cadien, and A. Y. Elezzabi, Appl. Phys. Lett. **99**, 253503 (2011).

[10]F. Aydinoglu, M. Alhazmi, B. Cui, O.M. Ramahi, M. Irannejad, A. Brzezinski, and M. Yavuz, Austin J Nanomed Nanotechnol. **1**(1), 3 (2014).

[11]A. Singh, R. Ratnadurai, R. Kumar, S. Krishnan, Y. Emirov, and S. Bhansali, Appl. Surf. Sci. **334**, 197 (2015).

[12]A.D. Weerakkody, N. Sedghi, I.Z. Mitrovic, H. van Zalinge, I. Nemr Noureddine, S. Hall, J.S. Wrench, P.R. Chalker, L.J. Phillips, R. Treharne, and K. Durose, Microelectron. Eng. **147**, 298 (2015).

[13]I. Nemr Noureddine, N. Sedghi, I.Z. Mitrovic, and S. Hall, J. Vac. Sci. Techn. B **35**(1), 01A117 (2017).

[14]I.Z. Mitrovic, M. Althobaiti, A.D. Weerakkody, V.R. Dhanak, N. Sedghi, S. Hall, P.R. Chalker, D. Tsoutsou, and A. Dimoulas, J. Appl. Phys. **115**, 114102 (2014).

[15]R.G. Southwick, A. Sup, A. Jain, and W.B. Knowlton, IEEE Trans. Device Mater. Reliab. **11**(2), 236 (2011).

[16]N. Alimardani, S.W. King, B.L. French, C. Tan, B.P. Lampert, and J.F. Conley Jr., J. Appl. Phys. **116**, 024508 (2014).

[17]E. Kraut, R. Grant, J. Waldrop, and S. Kowalczyk, Phys. Rev. Lett. **44**, 1620 (1980).

[18]E.E. Cowell III, N. Alimardani, C.C. Knutson, J.F. Conley Jr., D.A. Keszler, B.J. Gibbons, and J.F. Wager, Adv. Mater. **23**(1), 74 (2011).

[19]M.L. Huang, Y.C. Chang, C.H. Chang, T.D. Lin, J. Kwo, T.B. Wu, and M. Hong, Appl. Phys. Lett. **89**, 012903 (2006).

[20]S. Zaima, T. Furuta, Y. Koide, Y. Yasudo, and M. Iida, J. Electrochem. Soc. **137**, 2876 (1990).

[21]B.C. Lai, N. Kung, and J.Y. Lee, J. Appl. Phys. **85**, 4087 (1999).

[22]E.N. Grossman, T.E. Harvey, and C.D. Reintsema, J. Appl. Phys. **91**(12), 10134 (2002).

[23]M. Di Ventra, G. Papp, C. Coluzza, A. Baldereschi, and P. A. Schulz, J. Appl. Phys. **80**(7), 4174 (1996).

[24]C. Jirauschek, IEEE J. Quant. Electron. **45**(9), 1059 (2009).

[25]I.E. Hashem, N.H. Rafat, and E.A. Soliman, IEEE J. Quant. Electron. **49**(1), 72 (2013).

[26]A. K.Ghatak, K. Thyagarajan, and M. R. Shenoy, IEEE J. Quant. Electron. **24**, 1524 (1988).

[27]N. Sedghi, J. F. Ralph, I. Z. Mitrovic, P. R. Chalker, and S. Hall, Appl. Phys. Lett. **102**, 092103 (2013).

[28]N. Sedghi, J. W. Zhang, J. F. Ralph, Y. Huang, I. Z. Mitrovic, and S. Hall, in *Proc. 43rd European Solid-State Device Research Conference (ESSDERC 2013)*, pp. 131-134 (2013).

[29]R. Tsu and L. Esaki, Appl. Phys. Lett. **22**, 562 (1973).

[30]K. M. S. V. Bandara and D. D. Coon, J. Appl. Phys. **66**, 693 (1989).

[31]T. C. L. G. Sollner, W. D. Goodhue, P. E. Tannenwald, C. D. Parker, and D. D. Peck, Appl. Phys. Lett. **43**, 588 (1983).

[32]A.D. Weerakkody, *PhD thesis*, University of Liverpool, UK, 2016.

Figure Captions

FIG. 1 (a) X-ray photoelectron intensity spectra of secondary electrons cut-off and VBM measured from bulk Al_2O_3 (top) and Nb_2O_5 (bottom) samples. (b) XPS spectra of Nb 3d and Al 2p CLs for bulk Nb_2O_5 (top), interfacial 3.8 nm Nb_2O_5/Al_2O_3 (middle) and bulk Al_2O_3 samples. In addition, VB regions are shown, depicting extraction of VBM values for bulk Nb_2O_5 (top, right) and bulk Al_2O_3 (bottom, right) samples. The values derived from graphs are used to determine in: (a) electron affinities of oxides, and (b) VBO of Nb_2O_5/Al_2O_3 using Kraut's method. The thickness of bulk samples is > 10 nm.

FIG. 2 (a) Experimental and linearly fitted Fowler-Nordheim plots for reference Nb_2O_5- (left) and Ta_2O_5- (right) based MIM capacitors, with metal electrodes: Nb, Ag and Al. The values of M/I barrier heights extracted from linear fitting is depicted in the insets of each figure. The experimental graphs presented refer to the current-voltage curves when injection from the top metal electrodes is considered. If injection from the same metal bottom electrode is considered, the variation of extracted barrier heights from referring FN plots is ± 0.08 eV for Al-based, and ± 0.02 eV for Nb- and Ag-based MIM devices. (b) A graphical representation on energy scale of: work function values for Nb, Ag, and Al; electron affinities for Nb_2O_5 and Al_2O_3 as well as Nb_2O_5/Al_2O_3 valence band offset obtained in this work.

FIG. 3 Band diagrams for Nb/4 nm Nb_2O_5/1 nm Al_2O_3/Nb MI^2M structure for applied external bias of (a) 0.5 V and (b) 1 V. The values for barrier heights were taken from experimental data summarized in Fig. 2(b), i.e. $\phi(Nb/Nb_2O_5)$ = 0.39 eV; $CBO(Nb_2O_5/Al_2O_3)$ = 2.15 eV. The tunneling probability and transmittance curves derived using the theoretical model and assuming the band alignment in (a)-(b) for two cases of external biases: (c) ± 0.5 V, and (d) ± 1 V. The dashed horizontal lines in (a) and (b) refer to two bound states predicted by the model, further pointed by arrows on tunneling probability curves in (c) and (d) respectively. (Notation for curves in (c) and (d): full lines refer to external bias of 0.5 V, while dashed lines to –0.5 V; black lines refer to tunneling probability, while gray lines to transmittance.)

FIG. 4 (a) Experimental JV characteristics of Nb_2O_5/Al_2O_3 MI^2M devices with similar (Nb/Nb) and dissimilar (Nb/Ag) electrodes. The insets in both graphs refer to log J scale and cross-section of devices with nominal oxide thicknesses. The arrows depict the rectification reversal point where forward current starts to dominate reverse current, likely to be due to resonant tunneling. Note a clear shift of rectification reversal point to ~ 0.2 eV towards higher voltages due to the effect of Nb/Ag work function difference. (b)-(c) Asymmetry and responsivity graphs derived from (a) for referring MI^2M devices.

FIG. 5 Band diagrams of Nb/Nb_2O_5/Al_2O_3/Ag rectifier device under: (a) zero, (b)-(e) positive, and (f)-(g) negative bias. The thickness of the stack is 4.5 nm Nb_2O_5/1.1 nm Al_2O_3 measured by VASE. DT, FNT, RT and ST refer to direct, Fowler-Nordheim, resonant and step tunneling conduction mechanisms respectively identified for the stack under different bias conditions (c)-(g). The bias (electric field) across each insulator was calculated using a series capacitor model and thickness/permittivity of 25/4.5 nm for Nb_2O_5 and 10/1.1 nm for Al_2O_3.

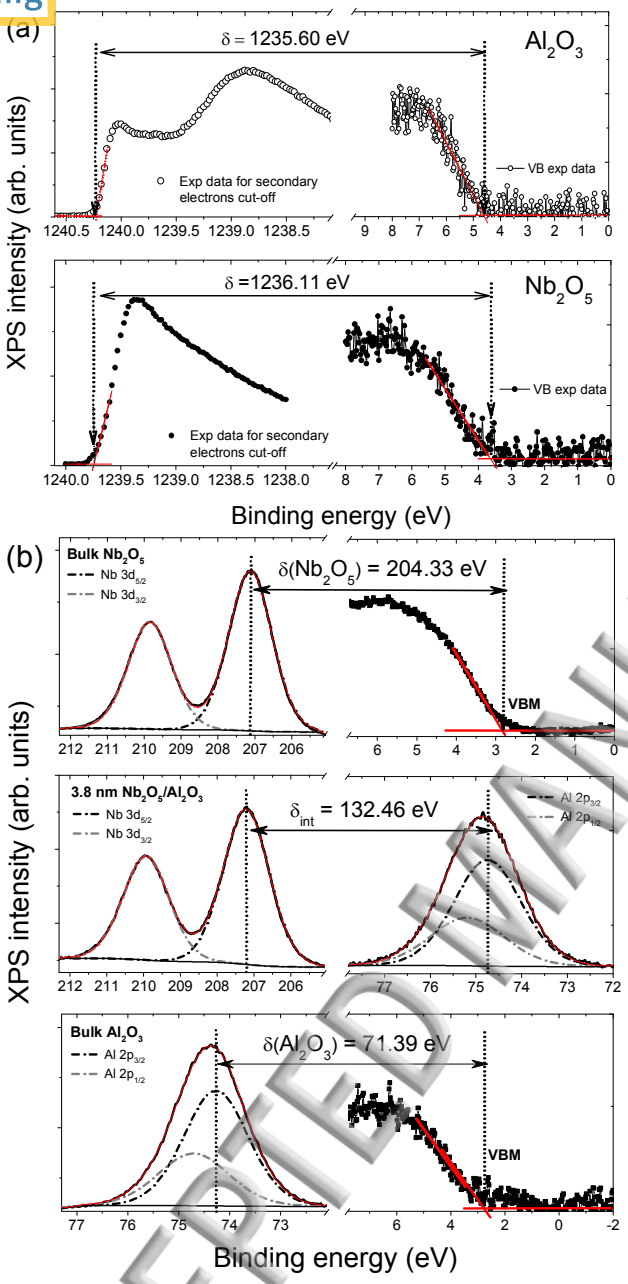

FIG. 1

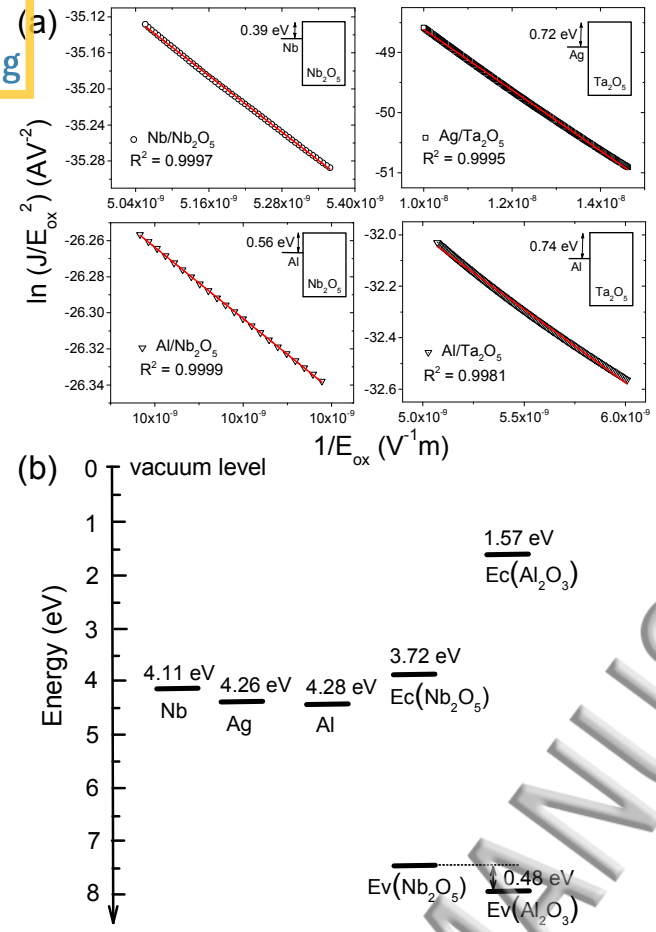

FIG. 2

This manuscript was accepted by Appl. Phys. Lett. Click here to see the version of record.

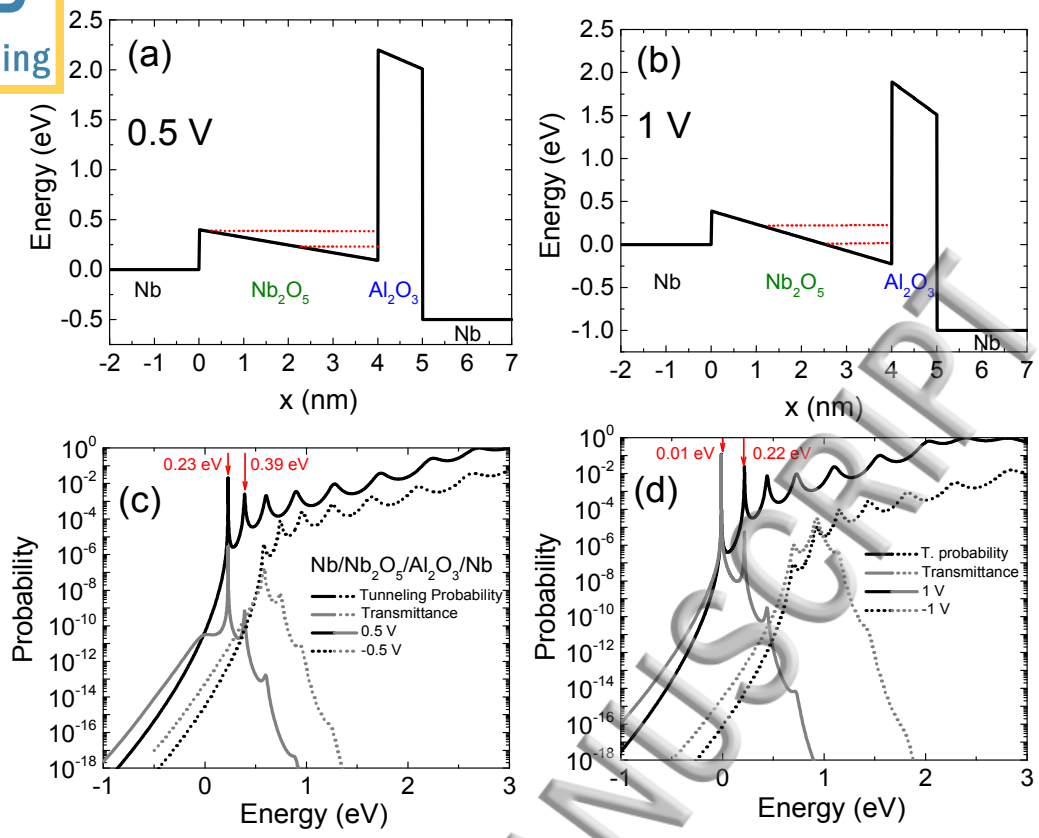

FIG. 3

This manuscript was accepted by Appl. Phys. Lett. Click here to see the version of record.

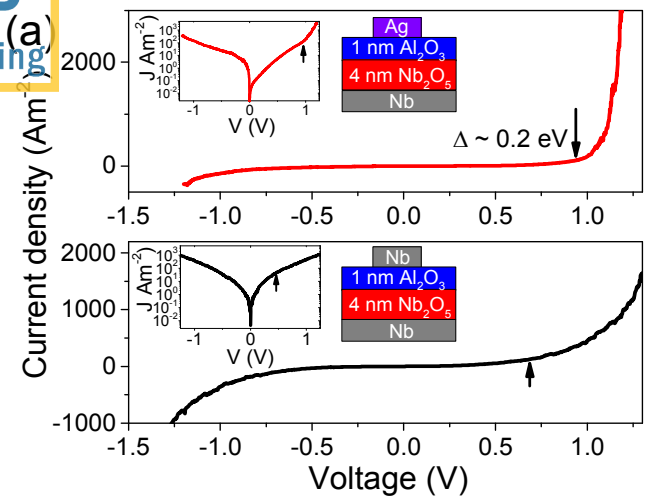

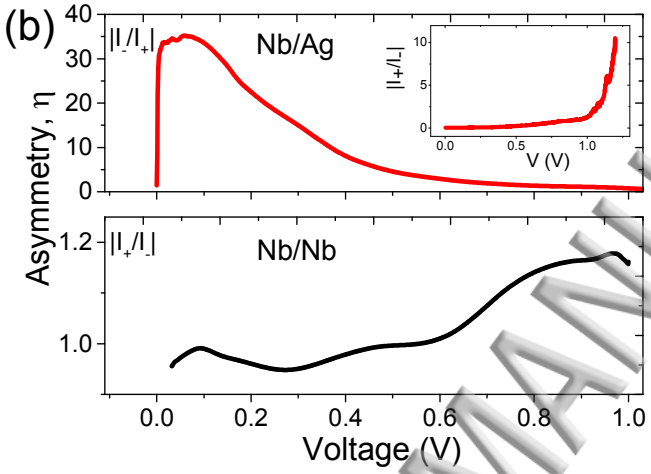

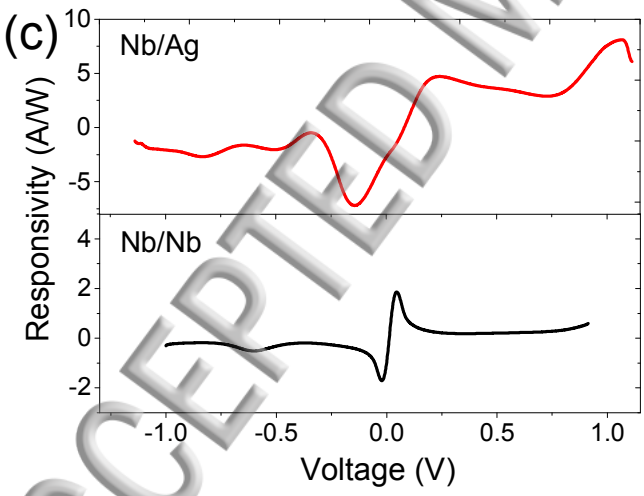

FIG. 4

This manuscript was accepted by Appl. Phys. Lett. Click here to see the version of record.

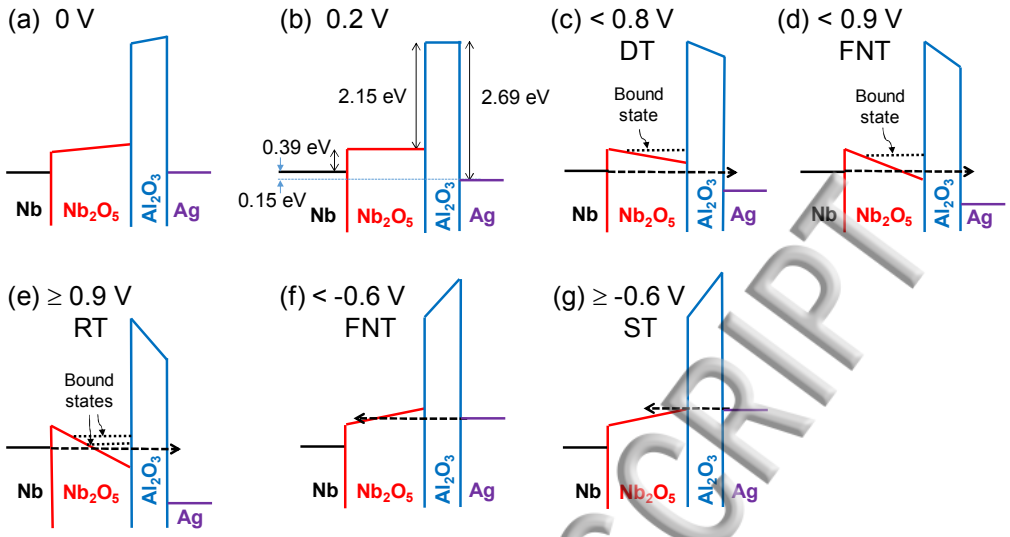

FIG. 5